Feng, Hai L., Kang, Chang-Jong, Manuel, Pascal, Orlandi, Fabio, Su, Yu, Chen, Jie, Tsujimoto, Yoshihiro, Hadermann, Joke, Kotliar, Gabriel, Yamaura, Kazunari and others (2021) *Antiferromagnetic Order Breaks Inversion Symmetry in a Metallic Double Perovskite, Pb2NiOsO6.* Chemistry of Materials . ISSN 0897-4756.

CHEMISTRY OF MATERIALS

Article

Antiferromagnetic Order Breaks Inversion Symmetry in a Metallic Double Perovskite, Pb$_2$NiOsO$_6$

Hai L. Feng,[††] Chang-Jong Kang,[††] Pascal Manuel, Fabio Orlandi, Yu Su, Jie Chen, Yoshihiro Tsujimoto, Joke Hadermann, Gabriel Kotliar, Kazunari Yamaura, Emma E. McCabe,* and Martha Greenblatt*

Cite This: https://doi.org/10.1021/acs.chemmater.1c01032

Read Online

ACCESS | Metrics & More | Article Recommendations | Supporting Information

ABSTRACT: A polycrystalline sample of Pb$_2$NiOsO$_6$ was synthesized under high-pressure (6 GPa) and high-temperature (1575 K) conditions. Pb$_2$NiOsO$_6$ crystallizes in a monoclinic double perovskite structure with a centrosymmetric space group $P2_1/n$ at room temperature. Pb$_2$NiOsO$_6$ is metallic down to 2 K and shows a single antiferromagnetic (AFM) transition at T_N = 58 K. Pb$_2$NiOsO$_6$ is a new example of a metallic and AFM oxide with three-dimensional connectivity. Neutron powder diffraction and first-principles calculation studies indicate that both Ni and Os moments are ordered below T_N and the AFM magnetic order breaks inversion symmetry. This loss of inversion symmetry driven by AFM order is unusual in metallic systems, and the 3d−5d double-perovskite oxides represent a new class of noncentrosymmetric AFM metallic oxides.
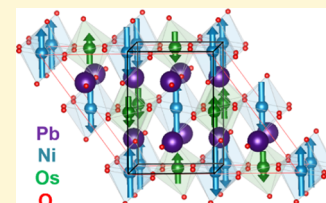
1. INTRODUCTION

Transition-metal oxides (TMOs) exhibit unique correlations between magnetism and electrical conductivity: ferromagnetism (FM) in TMOs usually coexists with metallic conductivity, whereas insulating TMOs usually exhibit antiferromagnetism (AFM).[1] Exceptions from this behavior, such as FM insulating oxides and AFM metallic oxides, are less common. CaCrO$_3$ and Nb$_{12}$O$_{29}$ are examples of AFM metallic oxides with three-dimensional crystal structures.[2−4] Other AFM metallic oxides such as La$_{2−2x}$Sr$_{1+2x}$Mn$_2$O$_7$ and Ca$_3$Ru$_2$O$_7$ crystallize in layered crystal structures, and FM couplings are dominant within the layer.[5,6] Recently, RuO$_2$, and LaNiO$_3$, which had been described as paramagnetic metals, were found to be AFM-ordered and are new examples of AFM metallic oxides with three-dimensional crystal and electronic structures.[7−9]

5d TMOs are unique correlated systems because of the spatial extent of the 5d electrons, generally giving 5d TMOs wider bandwidths (W), stronger spin−orbit coupling (SOC), and smaller on-site Coulomb repulsion (U) compared with 3d TMOs.[10] For instance, metal−insulator transitions driven by AFM orders were proposed in 5d oxides, Pb$_2$CaOsO$_6$,[11] Cd$_2$Os$_2$O$_7$,[12,13] and NaOsO$_3$,[14] and a ferroelectric-like structural-transition-breaking inversion symmetry has been observed in metallic LiOsO$_3$.[15] Recent studies on a 5d metallic oxide Pb$_2$CoOsO$_6$ demonstrated that the AFM order breaks inversion symmetry.[16,17] In this work, we have built on this, synthesizing a new 5d hybrid double perovskite oxide Pb$_2$NiOsO$_6$, which is a new example of an AFM metallic oxide. Characterization using neutron powder diffraction (NPD) and property measurements suggest that the magnetic order breaks inversion symmetry (similar to reports on Pb$_2$CoOsO$_6$[16]). First-principles calculations confirm that both Ni and Os moments are ordered, allowing us to confirm the nature of the ground state (which has not been fully explored previously). The 3d−5d double-perovskite oxides establish a new class of noncentrosymmetric AFM metallic oxides, and our symmetry analysis of Pb$_2$NiOsO$_6$ explores how this understanding can be applied more widely to design new magnetoelectrics.

2. EXPERIMENTAL SECTION

Polycrystalline Pb$_2$NiOsO$_6$ was synthesized via a solid-state reaction from powders of PbO$_2$ (99%, Alfa), Os (99.95%, Heraeus Materials), NiO (99.997%, Alfa), and KClO$_4$ (99.99%, Alfa). The powders were thoroughly mixed in a stoichiometric ratio in an Ar-filled glovebox, followed by sealing in a Pt capsule. The Pt capsule was statically and isotropically compressed in a belt-type high-pressure apparatus (Kobe Steel, Ltd., Japan[18]), and a pressure of 6 GPa was applied while the capsule was heated at 1400 °C for 1 h, followed by quenching to room temperature in less than a minute. The pressure was then gradually released over several hours.

A dense and black polycrystalline pellet was obtained, and several pieces were cut out from it. A selected piece was finely ground for a synchrotron X-ray diffraction (SXRD) study, which was conducted in a large Debye−Scherrer camera in the BL15XU beamline, SPring-8, Japan.[19,20] The SXRD pattern was collected at room temperature, and the wavelength was confirmed to be 0.65298 Å by measurement of a standard material, CeO$_2$. The absorption coefficient was measured in the same line. The SXRD data were analyzed by the Rietveld method with the RIETAN-VENUS software.[21] The crystal structure was depicted by VESTA.[22]

 A

The electrical resistivity (ρ) of a polycrystalline pellet of Pb_2NiOsO_6 was measured by a four-point method at a gauge current of 0.1 mA in a physical property measurement system (PPMS, Quantum Design, Inc.). Electrical contacts were made with Pt wires and Ag paste in the longitudinal direction. The temperature dependence of the specific heat capacity (C_P) was measured in the same PPMS by a thermal relaxation method at temperatures between 2 and 300 K with Apiezon N grease thermally connecting the material to the holder stage.

The magnetic susceptibility (χ) of Pb_2NiOsO_6 powder was measured in a magnetic property measurement system (Quantum Design, Inc.). The measurement was conducted in field-cooled (FC) and zero-FC conditions in the temperature range between 2 and 390 K. The applied magnetic field was 10 kOe.

Time-of-flight NPD data were collected at the WISH diffrac-tometer (target station 2) at the ISIS Neutron and Muon Source.[23] For the NPD data collection, 3.26 g of Pb_2NiOsO_6 powder was placed in a 6 mm diameter cylindrical vanadium can under helium and sealed using indium wires. The sample was loaded into a helium cryostat and cooled to base temperature (1.5 K). A high-quality data set was collected at 1.5 K (~1 h, ~40 μA h), and shorter scans (~15 min, ~10 μA h) were collected every 2.5 K on warming to 100 K. A final higher-quality scan (~1 h, ~40 μA h) was collected at 98 K in the paramagnetic phase. Data were analyzed and Rietveld refinements carried out using TopasAcademic,[24,25] and the web-based ISO-DISTORT software[26] was used for symmetry analysis. Rietveld refinements for the antiferromagnetic system were carried out with a nuclear phase and a magnetic-only phase, with atomic displacement parameters (ADPs) for the magnetic sites constrained to be equal to those sites in the nuclear phase. A separate peak shape was refined for the magnetic-only phase.

The density functional theory (DFT) calculation was performed on Pb_2NiOsO_6 with the all-electron full-potential linearized augmented plane-wave method implemented in the WIEN2k code.[27] Generalized gradient approximation (GGA) of Perdew−Burke−Ernzerhof (PBE)[28] was used for the exchange−correlation functional. The SOC was taken into account in the second variation method. To consider the correlation effect, GGA + U was adopted within fully localized limits.[29,30] The on-site Coulombic interaction parameters U = 4 and 2 eV for Ni and Os, respectively, and the Hund's coupling J_H = 0.8 eV, which was shown to describe a similar compound, Ca_2NiOsO_6 properly.[31]

3. RESULTS

3.1. Crystal Structure. Room-temperature SPXD data of Pb_2NiOsO_6 were successfully refined in a monoclinic double perovskite structure with space group $P2_1/n$ (see Supporting Information) similar to that reported for Pb_2CoOsO_6,[16] Pb_2MnReO_6,[32] and Pb_2CoTeO_6.[33] Due to the weak X-ray scattering power of O (especially in the presence of strong scatterers Os and Pb), complementary NPD data were used to confirm this nuclear structure at 98 K. NPD data collected at 98 K (above T_N) are consistent with the SPXD results and can be well fitted with a model of $P2_1/n$ symmetry (see the Supporting Information). The Ni and Os ions occupy 2a and 2b sites, respectively. Allowing for antisite disorder in the model during the refinement (with constraints to maintain stoichiometry) revealed complete B-site ordering (100(6)%). Refinement of the occupancies of Pb and O sites (with a single global ADP) indicated that the material is very close to stoichiometric ($Pb_{1.940(1)}NiOsO_{5.90(1)}$). This stoichiometry was assumed for further analysis. Trace amounts of PbO_2 and NiO impurities were identified and included in the refinement (no Os impurity was detected). Final refined atomic parameters and selected bond lengths and angles are summarized in the Supporting Information. The bond valence sum calcula-tions[34,35] support the nominal Ni^{2+} and Os^{6+} oxidation states

(see the Supporting Information). The refined crystal structure is shown in Figure 1a, where the corner-linked NiO_6 and OsO_6

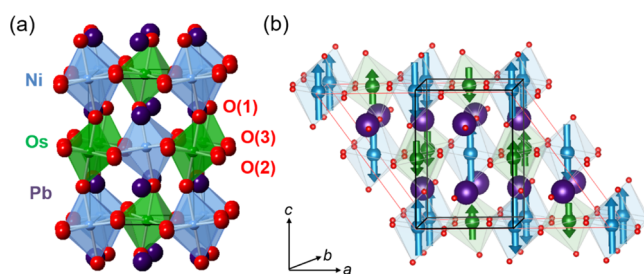**Figure 1.** Illustration of the nuclear (a) and magnetic structures (b) of Pb_2NiOsO_6 at 1.5 K from Rietveld refinement using NPD data; Pb, Ni, Os, and O sites are shown in purple, blue, green, and red, respectively; Ni and Os moments are shown by arrows. The nuclear unit cell is shown by solid black lines and the larger, monoclinic P_ac magnetic unit cell by solid red lines.

octahedra are ordered in the rock salt manner. The interoctahedral Ni−O−Os bond angles are 159.20(9), 161.3(4), and 160.5(4)°, which significantly deviate from 180° and imply substantial rotations of BO_6 octahedra.

3.2. Electrical and Magnetic Properties. The temper-ature dependence of resistivity (ρ) data decreases with cooling, as shown in Figure 2a, and shows the metallic nature of Pb_2NiOsO_6. The temperature dependence of magnetic susceptibility (χ) data shows a typical AFM transition with a peak at 58 K (see Figure 2b), which indicates the Néel
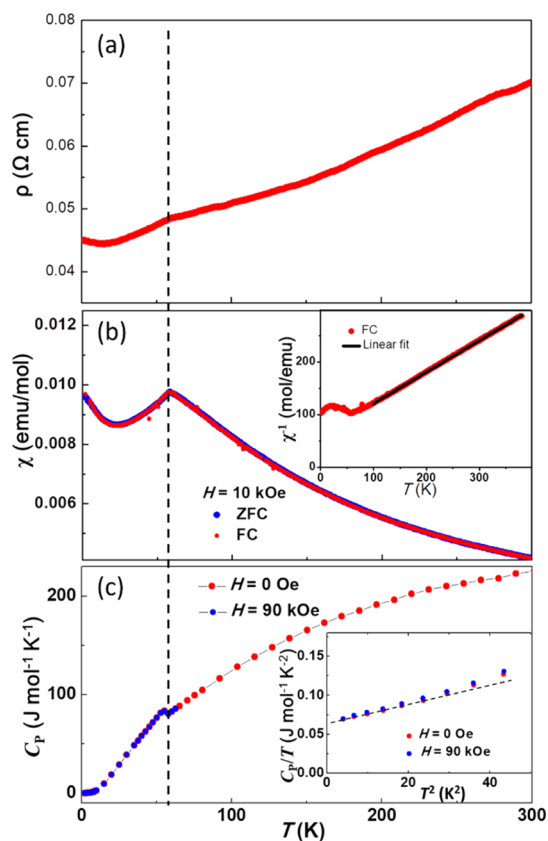
Figure 2. (a) Temperature-dependent resistivity, (b) temperature-dependent magnetic susceptibility, and (c) temperature-dependent specific heat of Pb_2NiOsO_6.
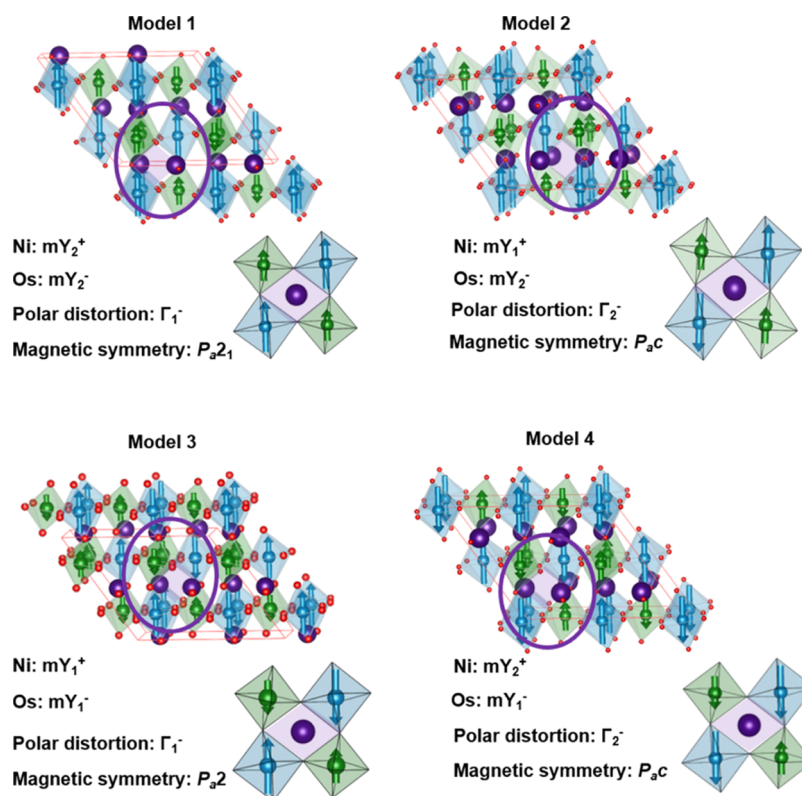
Figure 3. Four magnetic structures that result from the $k = (1/2\ 0\ 1/2)$ magnetic propagation vector for the $P2_1/n$ nuclear structure for Pb_2NiOsO_6 with a magnetic order on both Ni (blue) and Os (green) sites. To help visualize the difference between the four magnetic structures, the magnetic order around a PbO_{12} site (purple) viewed down the $[-1\ 1\ 0]$ direction of the nuclear unit cell is highlighted for each model. (Note that for model 2, the magnetic order around the PbO_{12} site is viewed along $[0\ -1\ 0]$ of the magnetic unit cell to show the magnetic moments about the same point in the nuclear structure).

temperature (T_N). The long-range AFM transition was further confirmed by specific heat data which display a λ-type anomaly at T_N (see Figure 2c). The χ^{-1} versus T data above the T_N show the Curie–Weiss behavior. Fitting the CW law to the data between 100 and 380 K results in an effective moment (μ_{eff}) of 3.66 μ_B per formula unit (f.u.) and a Weiss temperature (θ_W) of −102 K. The obtained effective moment is comparable to that in other Ni^{2+}–Os^{6+} double perovskites, 3.44 μ_B/f.u. for Sr_2NiOsO_6[36] and 3.46 μ_B/f.u. for Ba_2NiOsO_6.[37] These values are smaller than the spin-only moments of 4.0 μ_B per formula unit for the Ni^{2+} ($3d^8$: $S = 1$) and Os^{6+} ($5d^2$: $S = 1$), which may be due to the SOC of Os^{6+}. The negative θ_W corroborates that AFM interactions are dominant in Pb_2NiOsO_6, which is consistent with the AFM order. The low-temperature part of specific heat data is plotted in the C_P/T versus T^2, and the lowest temperature part can be characterized by an approximated Debye model ($C_P/T = \gamma + \beta_0 T^2$). The fitting gives a Sommerfeld coefficient (γ) of 63.5 mJ mol^{-1} K^{-2}. The large γ value is consistent with the metallic nature of Pb_2NiOsO_6. The deviation from linearity above 30 K^2 could be due to the lattice contribution.

3.3. Magnetic Structure. To study the magnetic structure of Pb_2NiOsO_6, NPD data were collected from 1.5 to 98 K. On cooling below 57 K, additional reflections were observed in NPD patterns, which increased smoothly in intensity on cooling (see the Supporting Information). These were consistent with magnetic ordering described by magnetic propagation vector $k = (1/2\ 0\ 1/2)$. As described for the double perovskites Pb_2CoOsO_6[16] and for the k_1 propagation vector for Sc_2NiMnO_6,[38] there are four irreps associated with

the magnetic propagation vector $k = (1/2\ 0\ 1/2)$: $mY_1^{\pm}$ and $mY_2^{\pm}$. The mY_n^+ (mY_n^-) irreps describe magnetic order on the Ni (Os) sites only. Magnetic susceptibility and heat capacity measurements for Pb_2NiOsO_6 (Figure 2b,c) and the evolution of magnetic Bragg intensity in NPD data collected on cooling (see the Supporting Information) suggest a single magnetic ordering transition which could result from one of three possible scenarios: (1) only Ni^{2+} moments order at T_N; (2) only Os^{6+} moments order at T_N or (3), both Ni^{2+} and Os^{6+} moments order simultaneously at T_N. As described for related double perovskites,[36,38−40] the magnetic moments on the two B sites are strongly correlated in refinements and NPD cannot unambiguously distinguish between these three scenarios. However, given the strong coupling between nearest Ni^{2+} and Os^{6+} ions in Ca_2NiOsO_6, it seems most likely that both Ni and Os sublattices order magnetically below T_N.[31] Experiments on Pb_2CoOsO_6 including muon spin rotation experiments support magnetic ordering of both Co^{2+} and Os^{6+} moments,[16] consistent with our analysis for Pb_2NiOsO_6. Mode inclusion analysis[41,42] using 1.5 K data suggested that the greatest improvement in fit was obtained with moments on the Os sites described by mY_2^- (R_{wp} decreased from 7.71% for a nonmagnetic model to 6.42% for the mY_2^- model) with Os moments close to the $[0\ 0\ 1]$ direction of the $P2_1/n$ nuclear unit cell. Magnetic ordering described by the mY_2^- irrep on the Os sites and the mY_1^+ (mY_2^+) irrep on the Ni sites breaks inversion symmetry, and the ferroelectric mode Γ_2^- (Γ_1^-) is coupled to both magnetic order parameters, allowing polar displacements in the ac plane ($[0\ 1\ 0]$ direction) of the $P2_1/n$ nuclear unit cell. These two possible structures are very similar,

and our NPD data do not allow us to confirm which is more appropriate to describe the low-temperature nuclear and magnetic structure of Pb_2NiOsO_6. Attempts to investigate the polar distortions using both NPD analysis and electron diffraction were not successful, suggesting that these distortions are very subtle. Consistent with DFT calculations (see below), the $mY_2^- \ mY_1^+ \ \Gamma_2^-$ model was assumed for all further analysis. This magnetic structure is described by the monoclinic unit cell of symmetry P_ac which is related to the $P2_1/n$ nuclear unit cell by the basis vectors $(-2\ 0\ 0)\ (0\ -1\ 0)\ (1\ 0\ 1)$ with an origin shift of $(0\ 1/4\ 0)$ (see Figure 1b). Given the complexity of the system, the moments on Ni and Os sites were constrained to be collinear (as observed in related systems[16,31,34,38−40,43]) and the moments on Os sites were constrained to be eight times smaller than those on Ni sites, as might be expected for Ni^{2+} (d^8) and Os^{6+} (d^2) with significant covalent bonding.[16,31,36,39] Allowing the moment direction to refine freely gave moments close to $[0\ 0\ 1]$ of the $P2_1/n$ nuclear unit cell, and constraining the moments to lie exactly along this direction gave a similar fit (R_{wp} was the same to three decimal places) and was used in subsequent analysis. Allowing ADPs to refine anisotropically did not give a significant improvement in fit and ADPs were found to be fairly isotropic. The final refinement profiles and parameters are given in the Supporting Information.

Sequential Rietveld refinements were carried out using NPD data collected on warming to study the evolution of nuclear and magnetic structures. The 1.5 K model described above was used, and this sequential analysis suggested a fairly smooth expansion of the structure on warming (see the Supporting Information).

3.4. First-Principles Calculations. DFT calculations were carried out to explore whether both Ni and Os moments are ordered in the magnetic phase of Pb_2NiOsO_6 and to differentiate between the possible magnetically ordered structures. First, the total energies were calculated for magnetic models with either AFM order on both Ni and Os sublattices or AFM order only on the Ni sublattice (see the Supporting Information). These calculations indicate that the model with the AFM order on both Ni and Os sublattices is 0.102 eV per formula unit more stable than that with only Ni-ordered moments. These calculations support the noncentrosymmetric AFM models in which both sublattices are ordered.

As discussed above, group theory calculations assuming the propagation vector $(1/2\ 0\ 1/2)$ and magnetic order on both Ni and Os sublattices (from magnetic irreps mY_1^+ and mY_2^+ on Ni sites, mY_1^- and mY_2^- on Os sites) give four possible isotropy subgroups (Figure 3). These models give comparable fits to the NPD data, and we are not able to unambiguously determine the magnetic ground state from our experimental work. Although the relative orientation of magnetic spins is similar in these four structures (they all have the ↑↑↓↓↑↑ sequence of moments on the Ni−Os chains along the $[0\ 0\ 1]$ direction of the nuclear unit cell), the superposition of the magnetic order on the nuclear structure (with monoclinic symmetry arising from rotations of NiO_6 and OsO_6 octahedra) results in different final symmetries and, as a consequence, in different distortions (e.g., polar degrees of freedom, bond distances, and angles) and hence different macroscopic properties.[44−46] Since the four models derive from different combinations of irreducible representations, these are distinct structures and not translational domains.

DFT calculations were carried out to differentiate between these similar magnetic structures and to determine the ground state. Calculations were carried out using the GGA(PBE) + SOC + U scheme to determine the energy of the four magnetic structures shown in Figure 3, and the relative energies are given in Table 1. Model 2 (described above from analysis of

Table 1. Total Energy and Magnetic Moment Calculated for Pb_2NiOsO_6 for Models Shown in Figure 3[a]

	energy (meV/atom)	total moment (μ_B)	spin moment (μ_B)	orbital moment (μ_B)
model 1	0	Ni: 1.85	Ni: 1.70	Ni: 0.15
		Os: 0.78	Os: 0.99	Os: −0.21
model 2	**−0.36**	**Ni: 1.86**	**Ni: 1.70**	**Ni: 0.16**
		Os: 0.78	**Os: 0.99**	**Os: -0.21**
model 3	+0.18	Ni: 1.85	Ni: 1.70	Ni: 0.15
		Os: 0.77	Os: 0.99	Os: −0.22
model 4	+0.42	Ni: 1.85	Ni: 1.70	Ni: 0.15
		Os: 0.76	Os: 0.99	Os: −0.23

[a]Unit of the energy is meV per atom and is calculated by dividing the DFT total energy by the number of atoms in the unit cell (40 for the magnetic unit cells shown in Figure 3). Model 1 is chosen as the reference energy. Details about magnetic moments are discussed in the main text.

NPD data, Figure 1b) is found to be the lowest in energy for calculations including SOC (Table 1). These results suggest that the ground state of Pb_2NiOsO_6 is best described by P_ac magnetic symmetry, with Γ_2^- polar degrees of freedom, consistent with the ground state reported for Pb_2CoOsO_6.[16] Notice that the same ground state was found for Pb_2NiOsO_6 from calculations without accounting for SOC. Mode decomposition of the relaxed structures from these DFT calculations was carried out using ISODISTORT,[26] but the amplitudes of polar displacements were very small (≤0.00035); this is consistent with NPD and electron diffraction analysis, both unable to confirm these displacements. The subtlety of these polar distortions (and that they are secondary rather than primary order parmeters) is born out by the fact that the two lowest energy structures (models 1 and 2) allow different polar distortions, suggesting that these distortions play a minor role in giving the noncentrosymmetric ground-state structure.

The electronic structure of Pb_2NiOsO_6 for model 2 (total and partial) is shown in Figure 4. Since Ni and Os atoms have local magnetic moments (Table 1), they show local spin polarization, as shown in Figure 4b,c. These local spin polarizations are summed to be zero, that is, the net total magnetic moment is zero, reflecting that Pb_2NiOsO_6 is antiferromagnetic, as demonstrated in Figure 4a.

The major contributions to the total DOS around the E_F are attributed to the Os 5d orbitals in both spin channels, which hybridize strongly with the O 2p orbitals. Occupation numbers for Ni 3d and Os 5d are 7.81 and 3.80, respectively. The huge hybridization indicated between Os 5d and O 2p orbitals suggests Ni^{2+} and Os^{6+} formal oxidation states in Pb_2NiOsO_6, consistent with the magnetic susceptibility experiment. Spin and orbital moments for Ni are 1.70 and 0.16 μ_B, respectively, thereby giving a total magnetic moment of 1.86 μ_B per Ni. For Os, spin and orbital moments are 0.99 and −0.21 μ_B, respectively, where the minus sign indicates that the orbital moment is opposite the spin direction; thus, the total moment is 0.78 μ_B per Os. These calculated moments are comparable
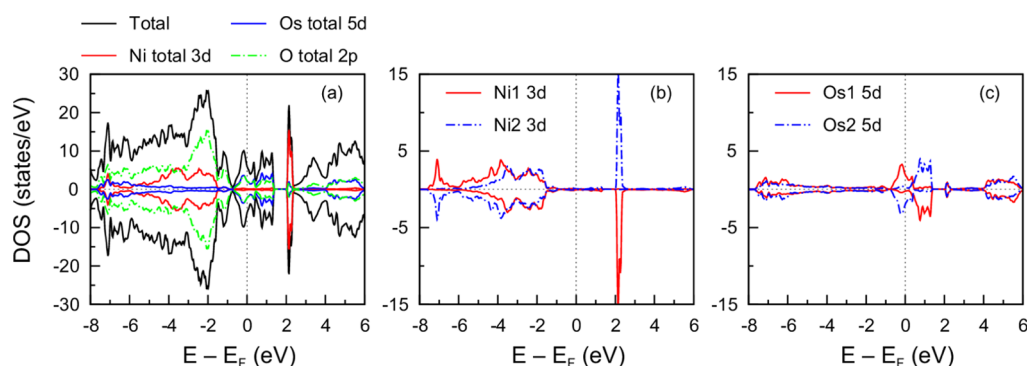
Figure 4. Total and partial density of states (PDOS) of Pb_2NiOsO_6 for model 2 from GGA + SOC + U calculation. (a) Black solid line corresponds to the total DOS. Red solid, blue solid, and green dashed dotted lines represent total Ni 3d, total Os 5d, and O 2p PDOS, respectively. (b) PDOS for each Ni 3d: Ni1 (Ni2) is presented for the spin majority as spin up (down). (c) PDOS for each Os 5d: Os1 (Os2) is presented for the spin majority as spin up (down). The positive and negative values in DOS correspond to spin up and down, respectively.

315 with those obtained from NPD analysis (see above). The
316 calculated γ is 7.1 mJ mol^{-1} K^{-2}. This is much smaller than the
317 one obtained from the fitting of low-temperature specific heat
318 data (63.5 mJ mol^{-1} K^{-2}), which may be due to the fact that
319 DFT underestimates the electronic correlations in the
320 correlated systems, resulting in a relatively small γ value.

4. DISCUSSION

321 The A_2NiOsO_6 (A = Ca^{2+}, Sr^{2+}, Ba^{2+}, and now Pb^{2+}) oxides
322 adopt B-site ordered double perovskite structures and span a
323 range of properties, from insulating (A = Ca[31]) to metallic (A
324 = Pb) and from ferromagnetic (A = Ba at low temperatures[37])
325 to antiferromagnetic (A = Sr[36]). While all these analogues
326 adopt the rocksalt ordering of NiO_6 and OsO_6 octahedra, the
327 degree of tilting of these octahedra increases with decreasing A
328 cation radius: Ba_2NiOsO_6 is cubic with 180° Ni−O−Os bond
329 angles; in tetragonal Sr_2NiOsO_6, octahedra are tilted around
330 the long axis, giving 180°/166° Ni−O−Os angles,[36] while
331 Ca_2NiOsO_6 adopts the monoclinic $P2_1/n$ structure (with
332 $a^-a^-c^+$ tilts) with Ni−O−Os angles of ∼151°.[36] Pb_2NiOsO_6
333 also adopts this $P2_1/n$ structure despite the ionic radius of Pb^{2+}
334 (1.49 Å) being comparable to that of Sr^{2+} (1.44 Å);[47] this
335 might in part be due to the inert pair Pb^{2+} ion favoring the
336 lower-symmetry coordination environment[48] possible in the
337 $P2_1/n$ structure: Pb occupies the 4e site of 1 symmetry in $P2_1/$
338 n compared with the higher-symmetry 4d site of −4 symmetry
339 in the $I4/m$ structure of Sr_2NiOsO_6.

340 The magnetic structure described here for Pb_2NiOsO_6 is of
341 the same symmetry as that reported for Pb_2CoOsO_6,[16]
342 although with a slightly different orientation of moments,
343 likely resulting from the different magnetic anisotropies of
344 Co^{2+} and Ni^{2+} ions in octahedral coordination environments.
345 In both Pb_2NiOsO_6 and Pb_2CoOsO_6, the magnetic order on
346 the Ni/Co and Os sublattices breaks inversion symmetry and
347 follows an ↑↑↓↓ sequence along [0 0 1] of the nuclear unit cell.
348 Magnetic ordering has been shown to break inversion
349 symmetry in other perovskites, including Sr_2NiMnO_6, but
350 with weak coupling between Ni and Mn sublattices,[38] in
351 contrast to Pb_2BOsO_6 (B = Co, Ni), which seem to have
352 collinear moments on both B and Os sublattices and a single
353 magnetic ordering transition. These observations are consistent
354 with strong couplings between Co/Ni and Os sublattices. This
355 ↑↑↓↓ magnetic structure observed in Pb_2NiOsO_6 is signifi-
356 cantly different from those reported for other A_2NiOsO_6
357 double perovskites. Previous works have highlighted the

358 importance of both nearest-neighbor (likely FM) and next-
359 nearest-neighbor (likely AFM) interactions in these sys-
360 tems.[31,49] The balance between these (competing) interactions
361 gives some magnetic frustration in Sr_2NiOsO_6 and makes the
362 magnetic structure of A_2NiOsO_6 phases very sensitive to bond
363 angles.[31]

364 The symmetry requirements for magnetic order to break
365 inversion symmetry have been explored by Perez-Mato et al.[50]
366 and provide a recipe for designing new magnetoelectrics. If the
367 magnetic k vector is not compatible with the screw axes or
368 glide planes of the nuclear (paramagnetic) unit cell (when time
369 reversal symmetry is considered), then full magnetic order on a
370 lattice of magnetic atoms on special sites (of −1 symmetry)
371 will break the inversion symmetry, resulting in noncentrosym-
372 metric structures.[50]

373 The double perovskites considered here have rocksalt
374 ordering of B and B′ cations on sites related by an origin
375 shift (and typically with symmetries including inversion
376 centers). If a single magnetic propagation vector k describes
377 the magnetically ordered phase, and full magnetic order is
378 expected on both B and B′ sublattices, then, depending on k,
379 the irreps to describe the magnetic order on each sublattice
380 may be of opposite parity with respect to an inversion center at
381 the origin. These irreps couple to a noncentrosymmetric
382 distortion (Γ_x^-), breaking inversion symmetry. This is the case
383 described here for Pb_2NiOsO_6 for k = (1/2 0 1/2) and also for
384 k = (−1 1/2 1/2). Likewise for a cubic double perovskite
385 $A_2BB'O_6$ of $Fm\bar{3}m$ nuclear symmetry (with magnetic B and B′
386 ions on 4a and 4b sites, respectively), a magnetic k = (1/2 1/2
387 1/2) would have a similar effect. This is also observed in the
388 hexagonal Ca_3CoMnO_6 ($R\bar{3}c$ nuclear symmetry, Mn^{3+} and
389 Co^{3+} ions on 6a (0 0 1/4) and 6b (0 0 0) sites, respectively)
390 with magnetic k = (0 0 0) giving the well-known ↑↑↓↓ polar
391 magnetic structure.[51]

392 If suitable cation-ordered structures with strong magnetic
393 coupling between the two sublattices (to favor them ordering
394 with the same magnetic k vector) can be identified, then new
395 magnetoelectrics might be designed if the magnetic exchange
396 interactions can be balanced to give the desired k vector. We
397 note that the improper ferroelectricity described here does not
398 require additional ordering of A-site cations (e.g., the
399 $AA'NiOsO_6$ phases explored recently).[52]

400 It is striking that both Pb_2NiOsO_6 and Pb_2CoOsO_6[16] are
401 metallic, in contrast to the SOC Mott-insulating nature of
402 Ca_2NiOsO_6 and Ca_2CoOsO_6,[31] despite the structural

similarities between these Pb and Ca analogues. First, we note that although Pb_2NiOsO_6 is metallic, its resistivity is several orders of magnitude higher than that of Pb_2CoOsO_6 (300 K resistivity is ~ 0.07 Ω cm (Figure 2a) and $\sim 3.5 \times 10^{-4}$ Ω cm for Ni and Co[16] analogues, respectively). This is similarly observed for Ca_2NiOsO_6 and Ca_2CoOsO_6 and is ascribed to the full occupancy of the Ni^{2+} t_{2g} band reducing delocalization of Os^{6+} t_{2g} electrons.[31]

The half-metallic nature proposed for Sr_2NiOsO_6 results from the partially-occupied Os t_{2g} states crossing the Fermi level, with SOC broadening the Os 5d bands.[53] This scenario can be applied to A_2NiOsO_6 (A = Ca, Pb), and our PDOS calculations (Figure 4) are qualitatively similar to those reported for Ca_2NiOsO_6[31] (with Ni t_{2g} states below ~ -2 eV and a narrow band of Ni e_g states at ~ 2 eV, with Os 5d and O 2p bands crossing E_F). However, the bandwidth in these double perovskites is also influenced by Ni–O–Os bond angles: in Ca_2NiOsO_6 with small Ca^{2+} ions, the Ni–O–Os angles (~ 149.3–$150.6°$ at 4 K)[36] show much larger deviations from the ideal $180°$ bond angles than in Pb_2NiOsO_6 (158.8–$161.0°$ at 1.5 K). The more distorted structure reported for the Ca analogues is likely to decrease the orbital overlap and bandwidth, giving wider band gaps than the less distorted Pb analogues. This is consistent with the insulating and more localized nature of Ca_2NiOsO_6 and its higher magnetic ordering temperature (158 K, compared with $T_N = 58$ K for Pb_2NiOsO_6).

5. CONCLUSIONS

A new 5d oxide Pb_2NiOsO_6 was synthesized under high pressure. Pb_2NiOsO_6 crystallizes in a monoclinic double perovskite structure with a centrosymmetric space group $P2_1/n$ at room temperature. Pb_2NiOsO_6 is metallic down to 2 K and displays an AFM transition with $T_N = 58$ K. Pb_2NiOsO_6 is a new example of AFM metallic oxides with three-dimensional crystal and electronic structures. NPD and DFT calculations indicate that both the Ni and Os moments are ordered below T_N, breaking inversion symmetry, which is similar to recently reported Pb_2CoOsO_6.[16,17] The magnetically driven loss of center of symmetry is similar to the type-II multiferroics. The discovery of 5d oxides Pb_2NiOsO_6 together with Pb_2CoOsO_6 establishes a new class of noncentrosymmetric AFM metallic oxides.

■ ASSOCIATED CONTENT

Ⓢ Supporting Information

The Supporting Information is available free of charge at https://pubs.acs.org/doi/10.1021/acs.chemmater.1c01032.

Refined room-temperature SXRD pattern and the corresponding crystal structure information, refined PND data at 98 and 1.5 K and the corresponding crystal structure information, evolution of nuclear and magnetic structures with temperature for Pb_2NiOsO_6 from sequential refinements using NPD data, and DFT calculations of Pb_2NiOsO_6 with different magnetic states (PDF)

■ AUTHOR INFORMATION

Corresponding Authors

Emma E. McCabe − *School of Physical Sciences, University of Kent, Canterbury, Kent CT2 7NH, U.K.; Department of Physics, Durham University, Durham DH1 3LE, U.K.;* orcid.org/0000-0001-5868-4570; Email: emma.mccabe@durham.ac.uk

Martha Greenblatt − *Department of Chemistry and Chemical Biology, Rutgers, the State University of New Jersey, Piscataway, New Jersey 08854, United States;* orcid.org/0000-0002-1806-2766; Email: greenbla@chem.rutgers.edu

Authors

Hai L. Feng − *Department of Chemistry and Chemical Biology, Rutgers, the State University of New Jersey, Piscataway, New Jersey 08854, United States; Beijing National Laboratory for Condensed Matter Physics and Institute of Physics, Chinese Academy of Sciences, Beijing 100190, China;* orcid.org/0000-0002-2699-3958

Chang-Jong Kang − *Department of Physics and Astronomy, Rutgers, the State University of New Jersey, Piscataway, New Jersey 08854, United States; Department of Physics, Chungnam National University, Daejeon 34134, South Korea;* orcid.org/0000-0003-2895-4888

Pascal Manuel − *ISIS Facility, STFC, Rutherford Appleton Laboratory, Didcot, Oxfordshire OX11 0QX, U.K.*

Fabio Orlandi − *ISIS Facility, STFC, Rutherford Appleton Laboratory, Didcot, Oxfordshire OX11 0QX, U.K.;* orcid.org/0000-0001-6333-521X

Yu Su − *International Center for Materials Nanoarchitectonics (WPI-MANA), National Institute for Materials Science, Tsukuba, Ibaraki 305-0044, Japan; Graduate School of Chemical Sciences and Engineering, Hokkaido University, Sapporo, Hokkaido 060-0810, Japan*

Jie Chen − *International Center for Materials Nanoarchitectonics (WPI-MANA), National Institute for Materials Science, Tsukuba, Ibaraki 305-0044, Japan; Graduate School of Chemical Sciences and Engineering, Hokkaido University, Sapporo, Hokkaido 060-0810, Japan;* orcid.org/0000-0001-9609-669X

Yoshihiro Tsujimoto − *International Center for Materials Nanoarchitectonics (WPI-MANA), National Institute for Materials Science, Tsukuba, Ibaraki 305-0044, Japan; Graduate School of Chemical Sciences and Engineering, Hokkaido University, Sapporo, Hokkaido 060-0810, Japan;* orcid.org/0000-0003-2140-3362

Joke Hadermann − *EMAT, University of Antwerp, 2020 Antwerp, Belgium;* orcid.org/0000-0002-1756-2566

Gabriel Kotliar − *Department of Physics and Astronomy, Rutgers, the State University of New Jersey, Piscataway, New Jersey 08854, United States*

Kazunari Yamaura − *International Center for Materials Nanoarchitectonics (WPI-MANA), National Institute for Materials Science, Tsukuba, Ibaraki 305-0044, Japan; Graduate School of Chemical Sciences and Engineering, Hokkaido University, Sapporo, Hokkaido 060-0810, Japan;* orcid.org/0000-0003-0390-8244

Complete contact information is available at:
https://pubs.acs.org/10.1021/acs.chemmater.1c01032

Author Contributions

††H.L.F. and C.-J.K. contributed equally.

Notes

The authors declare no competing financial interest.

■ ACKNOWLEDGMENTS

■ REFERENCES

(1) Goodenough, J. B. *Magnetism and the Chemical Bond*; Interscience Publisher, 1963; pp 165−275.

(2) Komarek, A. C.; Streltsov, S. V.; Isobe, M.; Moller, T.; Hoelzel, M.; Senyshyn, A.; Trots, D.; Fernandez-Diaz, M. T.; Hansen, T.; Gotou, H.; Yagi, T.; Ueda, Y.; Anisimov, V. I.; Grueninger, M.; Khomskii, D. I.; Braden, M. CaCrO3 An Anomalous Antiferromagnetic Metallic Oxide. *Phys. Rev. Lett.* **2008**, *101*, 167204.

(3) Cava, R. J.; Batlogg, B.; Krajewski, J. J.; Gammel, P.; Poulsen, H. F.; Peck, W. F.; Rupp, L. W. Antiferromagnetism and Metallic Conductivity in Nb12O29. *Nature* **1991**, *350*, 598−600.

(4) Cheng, J.-G.; Zhou, J.-S.; Goodenough, J. B.; Zhou, H. D.; Wiebe, C. R.; Takami, T.; Fuji, T. Spin Fluctuations in the Antiferromagnetic metal Nb12O29. *Phys. Rev. B: Condens. Matter Mater. Phys.* **2009**, *80*, 134428.

(5) Argyriou, D. N.; Mitchell, J. F.; Radaelli, P. G.; Bordallo, H. N.; Cox, D. E.; Medarde, M.; Jorgensen, J. D. Lattice effects and magnetic structure in the layered colossal magnetoresistance manganiteLa2−2xSr1+2xMn2O7, x=0.3. *Phys. Rev. B: Condens. Matter Mater. Phys.* **1999**, *59*, 8695−8702.

(6) Yoshida, Y.; Ikeda, S. I.; Matsuhata, H.; Shirakawa, N.; Lee, C. H.; Katano, S. Crystal and Magnetic Structure of Ca3Ru2O7. *Phys. Rev. B: Condens. Matter Mater. Phys.* **2005**, *72*, 054412.

(7) Berlijn, T.; Snijders, P. C.; Delaire, O.; Zhou, H. D.; Maier, T. A.; Cao, H. B.; Chi, S. X.; Matsuda, M.; Wang, Y.; Koehler, M. R.; Kent, P. R. C.; Weitering, H. H. Itinerant Antiferromagnetism in RuO2. *Phys. Rev. Lett.* **2017**, *118*, 077201.

(8) Zhu, Z. H.; Strempfer, J.; Rao, R. R.; Occhialini, C. A.; Pelliciari, J.; Choi, Y.; Kawaguchi, T.; You, H.; Mitchell, J. F.; Shao-Horn, Y.; Comin, R. Anomalous Antiferromagnetism in Metallic RuO2 Determined by Resonant X-Ray Scattering. *Phys. Rev. Lett.* **2019**, *122*, 017202.

(9) Guo, H.; Li, Z. W.; Zhao, L.; Hu, Z.; Chang, C. F.; Kuo, C. Y.; Schmidt, W.; Piovano, A.; Pi, T. W.; Sobolev, O.; Khomskii, D. I.; Tjeng, L. H.; Komarek, A. C. Antiferromagnetic Correlations in the Metallic Strongly Correlated Transition Metal Oxide LaNiO3. *Nat. Commun.* **2018**, *9*, 43.

(10) Witczak-Krempa, W.; Chen, G.; Kim, Y. B.; Balents, L. Correlated Quantum Phenomena in the Strong Spin-Orbit Regime. *Annu. Rev. Condens. Matter Phys.* **2014**, *5*, 57−82.

(11) Jackbsen, H.; Feng, H. L.; Princep, A. J.; Rahn, M. C.; Guo, Y.; Chen, J.; Matsushita, Y.; Tsujimoto, Y.; Nagao, M.; Khalyavin, D.; Manuel, P.; Murray, C. A.; Donnerer, C.; Vale, J. G.; Sala, M. M.; Yamaura, K.; Boothroyd, A. T. Magnetically Induced Metal-Insulator Transition in Pb2CaOsO6. *Phys. Rev. B* **2020**, *102*, 214409.

(12) Mandrus, D.; Thompson, J. R.; Gaal, R.; Forro, L.; Brayan, J. C.; Chakoumakos, B. C.; Woods, L. M.; Sales, B. C.; Fishman, R. S.; Keppns, V. Continuous Metal-Insulator Transition in the Pyrochlore Cd2Os2O7. *Phys. Rev. B: Condens. Matter Mater. Phys.* **2001**, *63*, 195104.

(13) Padilla, W. J.; Mandrus, D.; Basov, D. N. Searching for the Slater Transition in the Pyrochlore Cd2Os2O7 with Infrared Spectroscopy. *Phys. Rev. B: Condens. Matter Mater. Phys.* **2005**, *66*, 035120.

(14) Calder, S.; Garlea, V. O.; McMorrow, D. F.; Lumsden, M. D.; Stone, M. B.; Lang, J. C.; Kim, J.-W.; Schueter, J. A.; Shi, Y. G.; Yamaura, K.; Sun, Y. S.; Tsujimoto, Y.; Christianson, A. D. Magnetically Driven Metal-Insulator Transition in NaOsO3. *Phys. Rev. Lett.* **2012**, *108*, 257209.

(15) Shi, Y.; Guo, Y.; Wang, X.; Princep, A. J.; Khalyavin, D.; Manuel, P.; Michiue, Y.; Sato, A.; Tsuda, K.; Yu, S.; Arai, M.; Shirako, Y.; Akaogi, M.; Wang, N.; Yamaura, K.; Boothroyd, A. T. A Ferroelectric-like Structural Transition in a Metal. *Nat. Mater.* **2013**, *12*, 1024−1027.

(16) Princep, A. J.; Feng, H. L.; Guo, Y. F.; Lang, F.; Weng, H. M.; Manuel, P.; Khalyavin, D.; Senyshyn, A.; Rahn, M. C.; Yuan, Y. H.; Matsushita, Y.; Blundell, S. J.; Yamaura, K.; Boothroyd, A. T. Magnetically Driven Loss of Centrosymmetry in Metallic Pb2CoOsO6. *Phys. Rev. B* **2020**, *102*, 104410.

(17) Jiao, Y.; Fang, Y.-W.; Sun, J.; Shan, P.; Yu, Z.; Feng, H. L.; Wang, B.; Ma, H.; Uwatoko, Y.; Yamaura, K.; Guo, Y.; Chen, H.; Cheng, J. Coupled Magnetic and Structural Phase Transitions in the Antiferromagnetic Polar Metal Pb2CoOsO6 Under Pressure. *Phys. Rev. B* **2020**, *102*, 144418.

(18) Yamaura, K. Short Review of High-Pressure Crystal Growth and Magnetic and Electrical Properties of Solid-State Osmium Oxides. *J. Solid State Chem.* **2016**, *236*, 45−54.

(19) Tanaka, M.; Katsuya, Y.; Matsushita, Y.; Sakata, O. Development of a Synchrotron Powder Diffractometer with a One-Dimensional X-Ray Detector for Analysis of Advanced Materials. *J. Ceram. Soc. Jpn.* **2013**, *121*, 287−290.

(20) Tanaka, M.; Katsuya, Y.; Yamamoto, A. A New Large Radius Imaging Plate Camera for High-Resolution and High-Throughput Synchrotron X-Ray Powder Diffraction by Multiexposure Method. *Rev. Sci. Instrum.* **2008**, *79*, 075106.

(21) Izumi, F.; Ikeda, T. A Rietveld-Analysis Programm RIETAN-98 and its Applications to Zeolites. *Mater. Sci. Forum* **2000**, *321−324*, 198−205.

(22) Momma, K.; Izumi, F. VESTA 3 for Three-Dimensional Visualization of Crystal, Volumetric and Morphology data. *J. Appl. Crystallogr.* **2011**, *44*, 1272−1276.

(23) Chapon, L. C.; Manuel, P.; Radaelli, P. G.; Benson, C.; Perrott, L.; Ansell, S.; Rhodes, N. J.; Raspino, D.; Duxbury, D.; Spill, E.; Norris, J. Wish: The New Powder and Single Crystal Magnetic Diffractometer on the Second Target Station. *Neutron News* **2011**, *22*, 22−25.

(24) Coelho, A. A. Indexing of Powder Diffraction Patterns by Iterative Use of Singular Value Decomposition. *J. Appl. Crystallogr.* **2003**, *36*, 86−95.

(25) Coelho, A. A. *Topas Academic: General Profile and Structure Analysis Software for Powder Diffraction Data*; Bruker AXS: Karlsruhe, Germany, 2012.

(26) Campbell, B. J.; Stokes, H. T.; Tanner, D. E.; Hatch, D. M. ISODISPLACE: a web-based tool for exploring structural distortions. *J. Appl. Crystallogr.* **2006**, *39*, 607−614.

(27) Blaha, P.; Schwarz, K.; Madsen, G. K. H.; Kvasnicka, D.; Luitz, J. *WIEN2K, an Augmented Plane Wave + Local Orbitals Program for Calculating Crystal Properties*; Technische Universität Wien: Wien, Austria, 2001.

(28) Perdew, J. P.; Burke, K.; Ernzerhof, M. Generalized Gradient Approximation Made Simple. *Phys. Rev. Lett.* **1996**, *77*, 3865−3868.

(29) Anisimov, V. I.; Solovyev, I. V.; Korotin, M. A.; Czyżyk, M. T.; Sawatzky, G. A. Density-Functional Theory and Nio Photoemission Spectra. *Phys. Rev. B: Condens. Matter Mater. Phys.* **1993**, *48*, 16929−16934.

(30) Anisimov, V. I.; Aryasetiawan, F.; Lichtenstein, A. I. First-Principles Calculations of the Electronic Structure and Spectra of Strongly Correlated Systems: The LDA+U Method. *J. Phys.: Condens. Matter* **1997**, *9*, 767−808.

(31) Morrow, R.; Samanta, K.; Dasgupta, T. S.; Xiong, J.; Freeland, J. W.; Haskel, D.; Woodward, P. M. Magnetism in Ca2CoOsO6 and

Ca_2NiOsO_6: Unraveling the Mystery of Superexchange Interactions between 3d and 5d Ions. *Chem. Mater.* **2016**, *28*, 3666−3675.

(32) Ramesha, K.; Sebastian, L.; Eichhorn, B.; Gopalakrishnan, J. Perovskite and Pyrochlore Modifications of Pb_2MnReO_6: Synthesis, Structure, and Electronic Properties. *Chem. Mater.* **2003**, *15*, 668−674.

(33) Ivanov, S. A.; Nordblad, P.; Mathieu, R.; Tellgren, R.; Ritter, C. Structural and Magnetic Properties of the Ordered Perovskite Pb_2CoTeO_6. *Dalton Trans.* **2010**, *39*, 11136−11148.

(34) Brown, I. D.; Altermatt, D. Bond-valence parameters obtained from a systematic analysis of the Inorganic Crystal Structure Database. *Acta Crystallogr., Sect. B: Struct. Sci.* **1985**, *41*, 244−247.

(35) Brese, N. E.; O'Keeffe, M. Bond-Valence Parameters for Solids. *Acta Crystallogr., Sect. B: Struct. Sci.* **1991**, *47*, 192−197.

(36) Macquart, R.; Kim, S.-J.; Gemmill, W. R.; Stalick, J. K.; Lee, Y.; Vogt, T.; zur Loye, H.-C. Synthesis, Structure, and Magnetic Properties of Sr_2NiOsO_6 and Ca_2NiOsO_6: Two New Osmium-Containing Double Perovskites. *Inorg. Chem.* **2005**, *44*, 9676−9683.

(37) Feng, H. L.; Calder, S.; Ghimire, M. P.; Yuan, Y. H.; Shirako, Y.; Tsujimoto, Y.; Matsushita, Y.; Hu, Z. W.; Kuo, C. Y.; Tjeng, L. H.; Pi, T. W.; Soo, Y. L.; He, J. F.; Tanaka, M.; Katsuya, Y.; Richter, M.; Yamaura, K. Ba_2NiOsO_6: A Dirac-Mott Insulator with Ferromagnetism Near 100 K. *Phys. Rev. B* **2016**, *94*, 235158.

(38) Yi, W.; Princep, A. J.; Guo, Y.; Johnson, R. D.; Khalyavin, D.; Manuel, P.; Senyshyn, A.; Presniakov, I. A.; Sobolev, A. V.; Matsushita, Y.; Tanaka, M.; Belik, A. A.; Boothroyd, A. T. Sc_2NiMnO_6: a Double Perovskite with Magnetoelectric Response Driven by Multiple Magentic Orders. *Inorg. Chem.* **2015**, *54*, 8012−8021.

(39) Morrow, R.; Yan, J.; McGuire, M. A.; Freeland, J. W.; Haskel, D.; Woodward, P. M. Effects of Chemical Pressure on the Magnetic Ground States of the Osmate Double Perovskites $SrCaCoOsO_6$ and Ca_2CoOsO_6. *Phys. Rev. B: Condens. Matter Mater. Phys.* **2015**, *92*, 094435.

(40) Morrow, R.; Freeland, J. W.; Woodward, P. M. Probing the Links between Structure and Magnetism in $Sr_{2-x}Ca_xFeOsO_6$ Double Perovskites. *Inorg. Chem.* **2014**, *53*, 7983−7992.

(41) Tuxworth, A. J.; McCabe, E. E.; Free, D. G.; Clark, S. J.; Evans, J. S. O. Structural Characterization and Physical Properties of the New Transition Metal Oxyselenide $La_2O_2ZnSe_2$. *Inorg. Chem.* **2013**, *52*, 2078−2085.

(42) McCabe, E. E.; Stock, C.; Rodrigues, E. E.; Wills, A. S.; Taylor, J. W.; Evans, J. S. O. Weak Spin Interactions in Mott Insulating $La_2O_2Fe_2OSe_2$. *Phys. Rev. B: Condens. Matter Mater. Phys.* **2014**, *89*, No. 100402(R).

(43) Taylor, A. E.; Morrow, R.; Lumsden, M. D.; Calder, S.; Upton, M. H.; Kolesnikov, A. I.; Stone, M. B.; Fishman, R. S.; Paramekanti, A.; Woodward, P. M.; Christianson, A. D. Origin of Magnetic Excitation Gap in Double Perovskite Sr_2FeOsO_6. *Phys. Rev. B* **2018**, *98*, 214422.

(44) Khalyavin, D. D.; Salak, A. N.; Olekhnovich, N. M.; Pushkarev, A. V.; Radyush, Y. V.; Manuel, P.; Raevski, I. P.; Zheludkevich, M. L.; Ferreira, M. G. S. Polar and Antipolar Polymorphs of Metastable Perovskite $BiFe_{0.5}Sc_{0.5}O_3$. *Phys. Rev. B: Condens. Matter Mater. Phys.* **2014**, *89*, 174414.

(45) Prosandeev, S. A.; Khalyavin, D. D.; Raevski, I. P.; Salak, A. N.; Olekhnovich, N. M.; Pushkarev, A. V.; Radyush, Y. V. Complex Antipolar 2×4×22 Structure with Pnma Symmetry in $BiFeO_3$ and $BiFe_{1/2}Sc_{1/2}O_3$: First-Principles Calculations. *Phys. Rev. B: Condens. Matter Mater. Phys.* **2014**, *90*, 054110.

(46) Schoop, L. M.; Topp, A.; Lippmann, J.; Orlandi, F.; Müchler, L.; Vergniory, M. G.; Sun, Y.; Rost, A. W.; Duppel, V.; Krivenkov, M.; Sheoran, S.; Manuel, P.; Varykhalov, A.; Yan, B.; Kremer, R. K.; Ast, C. R.; Lotsch, B. V. Tunable Weyl and Dirac States in the Nonsymmorphic Compound CeSbTe. *Sci. Adv.* **2018**, *4*, No. eaar2317.

(47) Shannon, R. D. Revised Effective Ionic Radii and Systematic Studies of Interatomic Distances in Halides and Chalcogenides. *Acta Crystallogr., Sect. A: Cryst. Phys., Diffr., Theor. Gen. Crystallogr.* **1976**, *32*, 751−767.

(48) Walsh, A.; Payne, D. J.; Egdell, R. G.; Watson, G. W. Stereochemistry of Post-Transition Metal Oxides: Revision of the Classical Lone Pair Model. *Chem. Soc. Rev.* **2011**, *40*, 4455−4463.

(49) Tian, C.; Wibowo, A. C.; zur Loye, H.-C.; Whangbo, M.-H. On the Magnetic Insulating States, Spin Frustration, and Dominant Spin Exchange of the Ordered Double-Perovskites Sr_2CuOsO_6 and Sr_2NiOsO_6: Density Functional Analysis. *Inorg. Chem.* **2011**, *50*, 4142−4148.

(50) Perez-Mato, J. M.; Gallego, S. V.; Elcoro, L.; Tasci, E.; Aroyo, M. I. Symmetry Conditions for Type II Multiferroicity in Commensurate Magnetic Structures. *J. Phys.: Condens. Matter* **2016**, *28*, 286001.

(51) Choi, Y. J.; Yi, H. T.; Lee, S.; Huang, Q.; Kiryukhin, V.; Cheong, S.-W. Ferroelectricity in an Ising Chain Magnet. *Phys. Rev. Lett.* **2008**, *100*, 047601.

(52) Shaikh, M.; Fathima, A.; Swamynadhan, M. J.; Das, H.; Ghosh, S. Investigation into Cation-Ordered Magnetic Polar Double Perovskite Oxides. *Chem. Mater.* **2021**, *33*, 1594−1606.

(53) Ghimire, M. P.; Hu, X. Compensated Half Metallicity in Osmium Double Perovskite Driven by Doping Effects. *Mater. Res. Express* **2016**, *3*, 106107.

(54) Gong, S.; Guo, S.-D.; Chen, P.; Liu, B.-G. Oxygen-Octahedral Distortion and Electronic Correlation Induced Semiconductor Gaps in Ferrimagnetic Double Perovskite Ca_2MReO_6 (M = Cr, Fe). *RSC Adv.* **2015**, *5*, 63165−63174.